CHAPTER 1

Modelling the Milk-Ejection Reflex

Gareth Leng[1] *and Jianfeng Feng*[2]

[1]Centre for Integrative Physiology, University of Edinburgh, George Square Edinburgh, EH8 9XDUK
[2]Department of Computer Science, University of Warwick, Coventry CV4 7ALUK

When babies suckle at a mother's breast, they are rewarded intermittently with a let-down of milk that results from secretion of *oxytocin (video 1)*. Oxytocin is synthesised by magnocellular neurons in the hypothalamus, and is packaged in neurosecretory vesicles. Each oxytocin neuron has one axon which projects into the *neurohypophysis* where it gives rise to about 2,000 nerve endings, all filled with vesicles. Oxytocin is secreted from these in response to action potentials (spikes), generated in the cell bodies and propagated down the axon. Normally, spiking is slow and asynchronous, but during suckling, every few minutes, each neuron discharges a burst of spikes that results in a large pulse of oxytocin. This *milk-ejection reflex* involves a positive feedback affecting the excitability of the oxytocin cells, and a negative feedback that 'spaces' the bursts. These involve the *dendrites* of oxytocin cells. Dendrites are where neurons receive afferent inputs, but are also the sites of release of factors that influence neuronal excitability. Dendritic secretion has both *autocrine effects* (on the cell of origin) and *paracrine effects* (on adjacent cells); it can occur in response to spike activity, but can also be triggered by stimuli that mobilise intracellular Ca^{2+} stores. Here we show how synchronized bursting can arise in a neuronal network model that incorporates these features.

Video 1 The milk ejection reflex in conscious rats.

Title of Book, Xth edition. By X.X. Author, X.X. Author and X.X. Author.
© 20XX John Wiley & Sons, Ltd. Published 20XX by John Wiley & Sons, Ltd.

The milk-ejection reflex

Oxytocin is made in several thousand magnocellular neurons whose cell bodies mostly lie within the supraoptic nuclei and the paraventricular nuclei of the hypothalamus. Each of these neurons has just one axon, and this axon extends into the neurohypophysis, where it gives rise to about 2000 swellings and nerve endings. Spikes propagated down the axons cause some of these vesicles to fuse with the plasma membrane (*calcium-dependent exocytosis*) and release their contents into the extracellular space from where it enters the systemic circulation. Normally, oxytocin cells fire at 1-3 spikes/s, but during suckling, every 5 min or so, they all discharge a brief burst of 50-150 spikes in 1-3 s. These synchronised bursts result in the secretion of a pulse of oxytocin into the systemic circulation; when this pulse reaches the mammary gland a few seconds later, it causes cells of the mammary gland to abruptly release milk into a collecting duct from which it can be extracted by suckling.

The background activity of oxytocin cells is much the same in lactating rats as in non-lactating rats; the cells fire slowly, asynchronously, and nearly randomly. At first, suckling produces little change in this, except that slow firing cells tend to speed up slightly, while faster firing neurons slow down. However, after a few minutes of suckling, the first bursts occur; these are small and involve only some cells, but progressively more cells are recruited until all show intense bursts. Bursts are elicited *specifically* by the suckling stimulus; many other stimuli cause oxytocin secretion, but they produce a graded increase in electrical activity that is identical in lactating and non-lactating rats, and which does not entail bursting.

Milk-ejection bursts (Figure 1) vary in amplitude from cell to cell and according to the strength of the suckling, but they are quite consistent in their shape, especially from one burst to the next in any one cell.

The supraoptic nucleus

In each of the supraoptic nuclei there are about 2000 oxytocin cells (Figure 2), each cell has 2-5 dendrites, and each dendrite contains more than10,000 vesicles. The cells intercommunicate within "bundles" of 3-8 dendrites; in lactating rats, the bundles are separated from each other by glial enclosures (thin sheet-like processes of specialised astrocytes "wrap round" the bundles), but within each bundle the dendrites are directly apposed to each other. In basal conditions, dendritic oxytocin release is not much influenced by spike activity, but it can be evoked by stimuli that mobilize intracellular Ca^{2+}. When oxytocin is released, it depolarizes oxytocin cells; it also mobilizes Ca^{2+} from intracellular stores, promoting further release of oxytocin.

Priming

The mobilisation of Ca^{2+} can "prime" the dendritic stores of oxytocin, making them available for subsequent activity-dependent release (Figure 3). During suckling, dendritic oxytocin release is detected *before* any increase in the electrical activity of oxytocin cells, and before any increase in secretion from the neurohypophysis, so it seems that the suckling input primes the dendritic stores of oxytocin, making them available for activity-dependent release.

Endocannabinoids

Oxytocin cells modulate their afferent inputs by producing endocannabinoids (and other substances), which inhibit excitatory inputs presynaptically, and oxytocin itself suppresses inhibitory inputs by attenuating the effects of GABA.

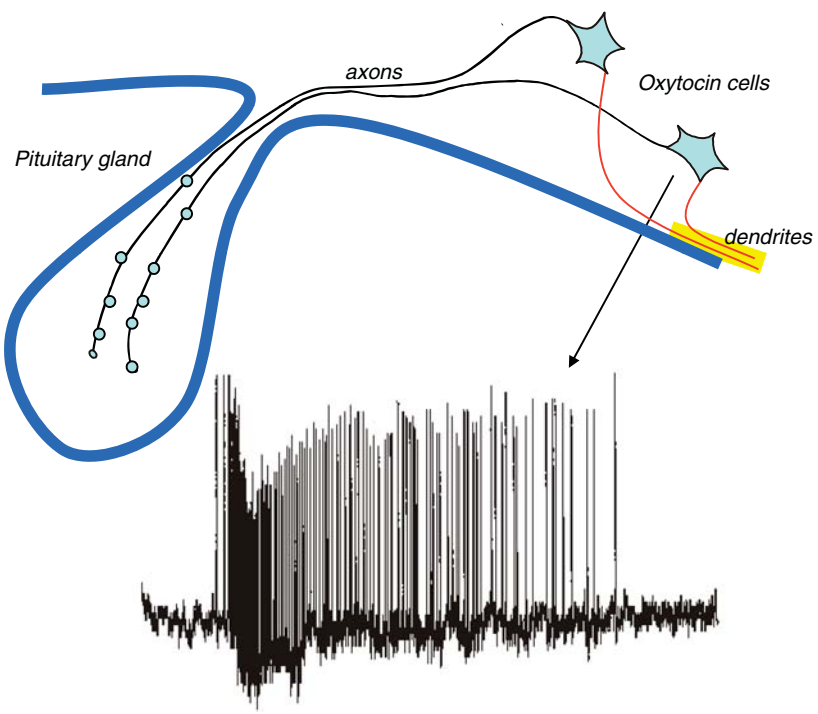

Figure 1 Milk-ejection bursts. Magnocellular oxytocin neurons each have one axon that projects into the neurohypophysis from where oxytocin is secreted into the general circulation. During suckling, they display intermittent high frequency bursts of spikes every few minutes. An example of one of these bursts is shown – the trace is a 2-s extract of a trace from an extracellular recording.

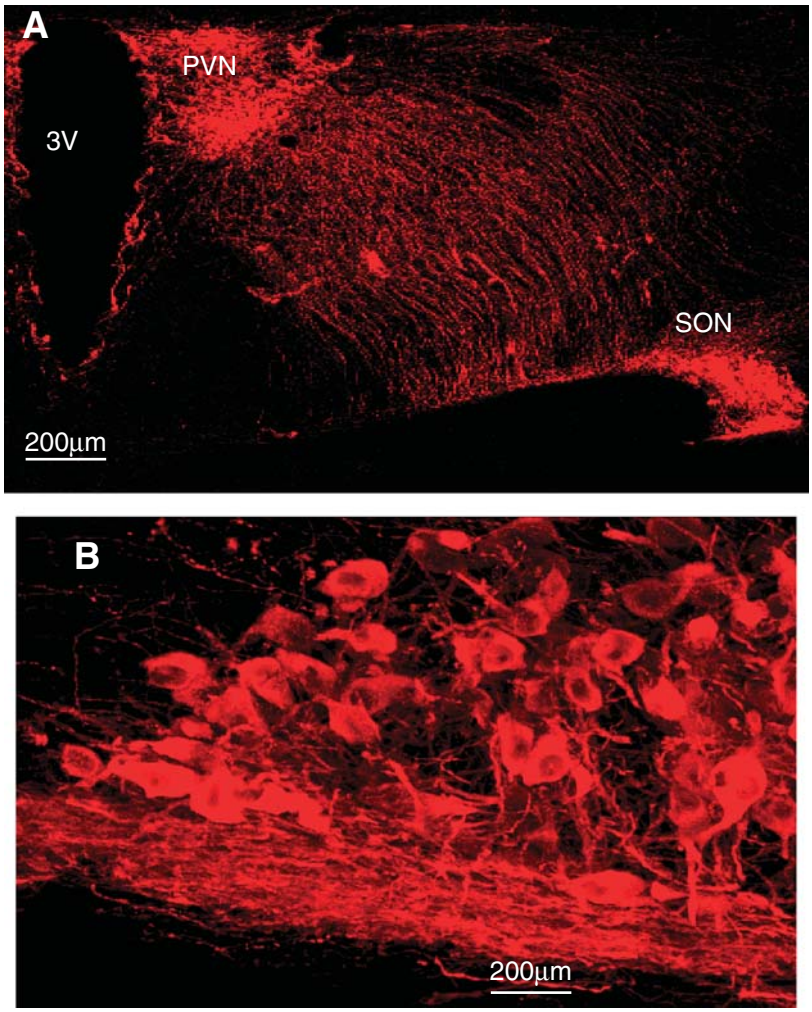

Figure 2 The supraoptic nucleus (SON) of the rat hypothalamus. A. Oxytocin cells in the SON and paraventricular nucleus (PVN) are stained red by immunohistochemistry, in a coronal section of the rat brain. 3V = third ventricle. B. Higher power view of the SON- the mat of fibres at the base of the nucleus are dendrites. Figure courtesy of Vicky Tobin.

Model

Mathematical modelling involves:

- *translating biological statements into differential equations or computational algorithms*
- *simulating a biological system by running these equations on a computer to generate "data" that can be compared with observational data*

- *"fitting" the model to observations by varying its parameters to ensure that the model data matches the real data*
- *"testing" the model by using it to generate new and unexpected predictions or insights*

Each model neuron is a *modified leaky integrate-and-fire model* (Figure 4), sometimes called a *spike-response model*. Such models describe a system that translates synaptic input (transient perturbations of voltage) into spikes, by a threshold function. They *integrate* synaptic inputs over time, calculating the cumulative balance of excitation and inhibition as deviations from a *resting potential*. A *leaky* model represents these perturbations as decaying towards the resting potential. A spike arises when the balance of input exceeds a spike threshold. A *modified* model, or *spike-response model*, incorporates activity-dependent changes in excitability to mimic the effects of slow voltage and calcium-dependent conductances; these may for example mimic hyperpolarising- or depolarising- after potentials that follow spikes.

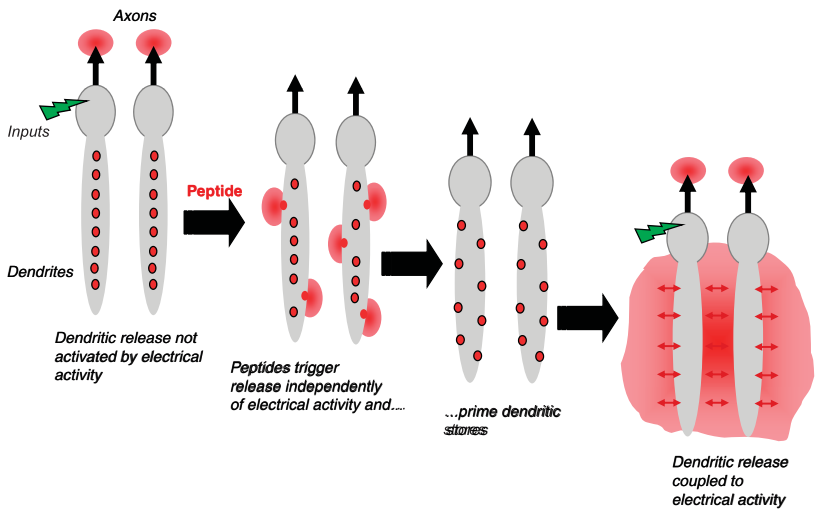

Figure 3 Priming in oxytocin cells. The dendrites of oxytocin cells contain many vesicles (shown as red organelles). These vesicles are normally located away from the plasma membrane, so stimuli that increase spike activity (indicated as a green stimulus) trigger release of oxytocin from axon terminals but not from dendrites. Some peptides can cause release from the dendrites without increasing spike activity, by triggering an increase in intracellular calcium release. In addition, some peptides can prime the dendritic stores – moving vesicles close to the plasma membrane. After priming, these vesicles are available for release in response to increases in spike activity.

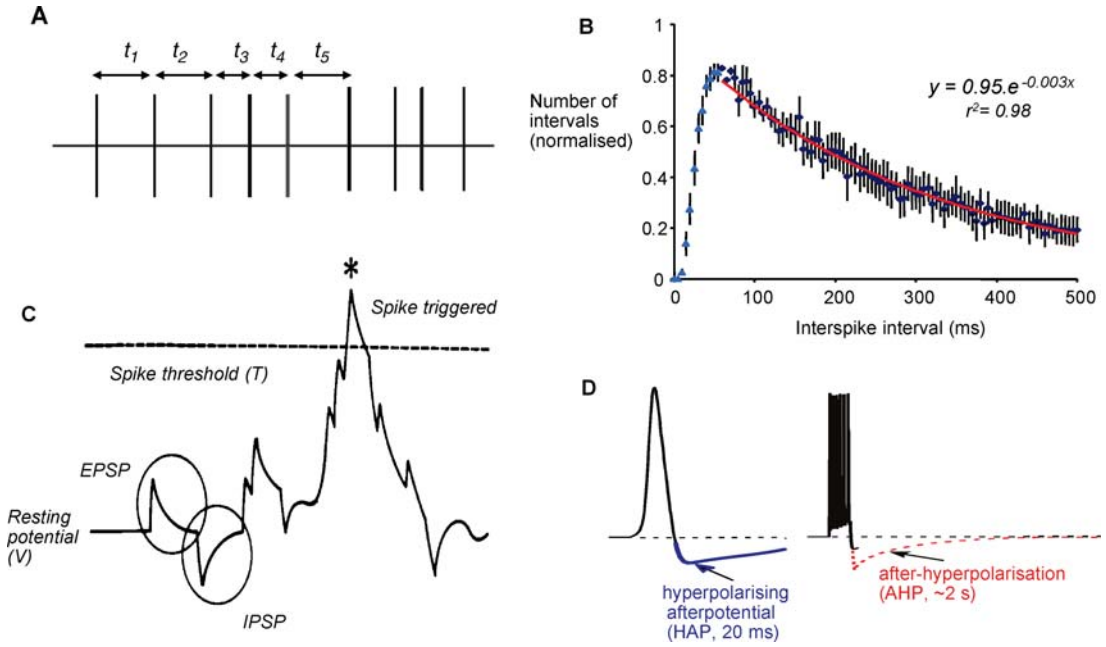

Figure 4 Spike activity in oxytocin cells. In background conditions, oxytocin cells discharge spikes at 1-3 spikes/s. This spiking can be characterised by measuring interspike intervals (*t1*, *t2* etc as shown in (**A**), and constructing an interspike interval histogram (**B**). Such histograms have a characteristic distribution – the tails of the histogram (for intervals > 50ms) can be well fitted by a single negative exponential (red line, fitted to average of 30 cells). From this, it appears that, after a spike, oxytocin cells have a relative refractory period of about 50 ms after which spikes arise approximately randomly. In the model, (**C**) spikes arise in model cells when incoming random EPSPs and IPSPs cause a fluctuation in resting potential sufficient to exceed a spike threshold. The relative refractoriness of oxytocin cells is the result of two post-spike hyperpolarising mechanisms (**D**) – a short but large HAP, and a smaller but longer acting AHP (which has a major effect only after bursts). In the model, these two mechanisms are modelled as transient changes in spike threshold that occur after each spike, rather than as changes in membrane potential – this is equivalent to changes in membrane potential, but computationally simpler to implement.

In the model described here, each oxytocin cell receives its own, random synaptic input. This is modelled as stochastic fast excitatory and inhibitory postsynaptic potentials (EPSPs and IPSPs, with realistic reversal potentials); in the model, this input is (normally) balanced, reflecting an equal average mixture of EPSPs and IPSPs (the neurons receive an approximately balanced synaptic input, mainly involving the neurotransmitters glutamate and GABA). The resting potential and spike threshold are fixed in line with measurements made *in vitro*, and the size and time course of EPSPs and IPSPs also match observations made *in vitro*. These inputs are not directly affected by suckling; they simply ensure that, in basal conditions, each cell has a different, irregular, level of background spiking activity.

Activity-dependent effects on excitability

After every spike, oxytocin cells are transiently refractory to excitation; this is because of a hyperpolarising afterpotential (HAP) that results from a Ca^{2+}-dependent K^+ conductance, and which follows spikes in oxytocin cells because spikes activate high threshold voltage-activated Ca^{2+} channels. This is modelled as a transient rise in spike threshold, and this alone is adequate for reproducing the characteristic distribution of interspike intervals *in vivo*.

Another modification mimics the effect of a slower activity-dependent afterhyperpolarisation (AHP). This is another Ca^{2+}-dependent K^+ conductance; it mediates a prolonged reduction in excitability after intense activation, and it is enhanced in oxytocin cells in lactation. This mechanism enables the model to fully reproduce the *shape* of milk-ejection bursts.

Dendritic oxytocin release

Oxytocin secretion from the neurohypophysis is facilitated at high spike frequencies, and this has been studied extensively. We assume that activity-dependent dendritic release is similarly non-linear, and so allow that dendritic oxytocin release only occurs when spikes occur with an interspike interval that is less than a critical value.

How much oxytocin is released depends on how much is available for release. In dendrites, only vesicles close to the plasma membrane (and hence close to voltage-gated Ca^{2+} channels) are released by spikes. This *readily-releasable pool* of vesicles is depleted when oxytocin is released and is replenished during suckling – the *priming* effects.

Dendro-Dendritic intercommunication

Oxytocin cells are interconnected via dendrites – each model cell is given two dendrites, each of which is part of a bundle that includes dendrites from other cells. Dendro-dendritic interactions are modelled by elements that mimic the excitatory actions of oxytocin, and this is implemented as an activity-dependent reduction in spike threshold that affects all the oxytocin cells that have

dendrites in the bundle where oxytocin is released. In the model, the maximum effect of oxytocin is limited to a depolarisation of 25 mV.

Endocannabinoid release

Oxytocin release is accompanied by production of endocannabinoids which feed back to modulate synaptic input. Endocannabinoids are produced in oxytocin cells as a consequence of the mobilisation of intracellular Ca^{2+}, and act via CB1 receptors on afferent nerve terminals. The rate of release of both EPSPs and IPSPs to all cells connected to a bundle is inhibited by the effects of endocannabinoids produced in that bundle.

Building the model

To model individual oxytocin cells, we use a *leaky integrate-and-fire model* **(**Figure 4**),** modified to incorporate activity-dependent changes in excitability.

Every cell in the model receives an independent synaptic input that is a mixture of EPSPs and IPSPs. These are represented by $N^j_{E,i}$, $N^j_{I,i}$ which are inhomogeneous Poisson processes of rate $\lambda^j_{E,i}(t)$, $\lambda^j_{I,i}(t)$, $a_E(v_E - v_{\text{rest}})$, $a_I(v_{\text{rest}} - v_I)$ are the magnitude of single EPSPs and IPSPs at v_{rest}, and v_E and v_I are the excitatory and inhibitory reversal potentials.

Spike generation

The membrane potential v_i of cell i obeys

$$\frac{dv_i}{dt} = \frac{v_{\text{rest}} - v_i}{\tau} + \sum_{j=1}^{2} \left[a_E(v_E - v_i) \frac{dN^j_{E,i}}{dt} - a_I(v_i - v_I) \frac{dN^j_{I,i}}{dt} \right] \tag{1}$$

where τ is the membrane time constant, and v_{rest} is the resting potential,

A spike is produced in cell i at time $t = t_i^s$, $s = 1, 2, \ldots,$ if $v_i(t_i^s) = T_i(t_i^s)$, where $T_i(t)$ is the spike threshold at time t. After the spike, v_i is reset to v_{rest}. Activity-dependent changes in excitability and the effects of oxytocin are modelled by effects on spike threshold:

$$T_i = T_0 + T_{HAP,i} + T_{AHP,i} - T_{OT,i} \tag{2}$$

where T_0 is a constant.

$T_{HAP,i}$ models the effect of a HAP in cell i by

$$T_{HAP,i} = k_{HAP} H(t - \hat{t}_i) e^{-(t-\hat{t}_i)/\tau_{HAP}} \tag{3}$$

where k_{HAP}, τ_{HAP} are constants, $\hat{t}_i = \max_s \{t_i^s : t_i^s \leq t\}$, and $H(x)$ is the Heaviside step function. This gives a transient increase in spike threshold after each spike.

Similarly, T_{AHP} models the effect of the AHP. The AHP builds up slowly, leading to a significant reduction of excitability only after intense activity. The variables $f_i, i = 1,\ldots,n$ represent the recent activity of each neuron, and

$$\frac{df_i}{dt} = -\frac{f_i}{\tau_{AHP}} + \sum_{t_i^s<t} \delta(t-t_i^s) \tag{4}$$

where τ_{AHP} is the decay constant of the AHP, and $\delta(x)$ is the Dirac delta function. We set

$$T_{AHP,i} = k_{AHP}\frac{f_i^4}{f_i^4+f_{th}^4} \tag{5}$$

where k_{AHP}, f_{th} are constants adjusted to match the characteristics of spontaneous firing in oxytocin cells.

Effects of oxytocin

The network topology (Figure 5) – the description of how cells are interconnected - is represented by matrices $C^k = \{C_{ij}^k\}$, $k = 1,\ldots, n$; $c_{ij}^k = 1$ if dendrite j of cell i is in bundle k, and zero otherwise. The increase in excitability due to oxytocin is modelled by T_{OT},

$$\frac{dT_{OT,i}}{dt} = -\frac{T_{OT,i}}{\tau_{OT}} + k_{OT}\sum_{k=1}^{n_b}\sum_{j=1}^{n}\sum_{l,m=1}^{2} c_{il}^k c_{jm}^k p_j^m(t) \tag{6}$$

where τ_{OT}, k_{OT} are constants, $p_j^m(t)$ is the release rate from dendrite m of cell j, and the sums pick up all the cells whose dendrites share the same bundle as cell i. The oxytocin-dependent reduction of the spike threshold is limited to a maximum ($T_{OT,max}$) of 25 mV.

Modelling oxytocin release from the dendrites

The readily-releasable pool of oxytocin in dendrite j of cell i is r_i^j, where

$$\frac{dr_i^j}{dt} = -\frac{r_i^j}{\tau_r} + k_p(t) - p_i^j(t), \tag{7}$$

where τ_r is a time constant, $k_p(t)$ is the rate of priming due to suckling ($k_p(t)$ is a positive constant during suckling and zero otherwise), and p_i^j is the instantaneous release rate from dendrite j. Release is proportional to the readily-releasable pool, so

$$p_i^j(t) = k_r r_i^j(t)\sum \delta(t-t_i^s-\Delta) \tag{8}$$

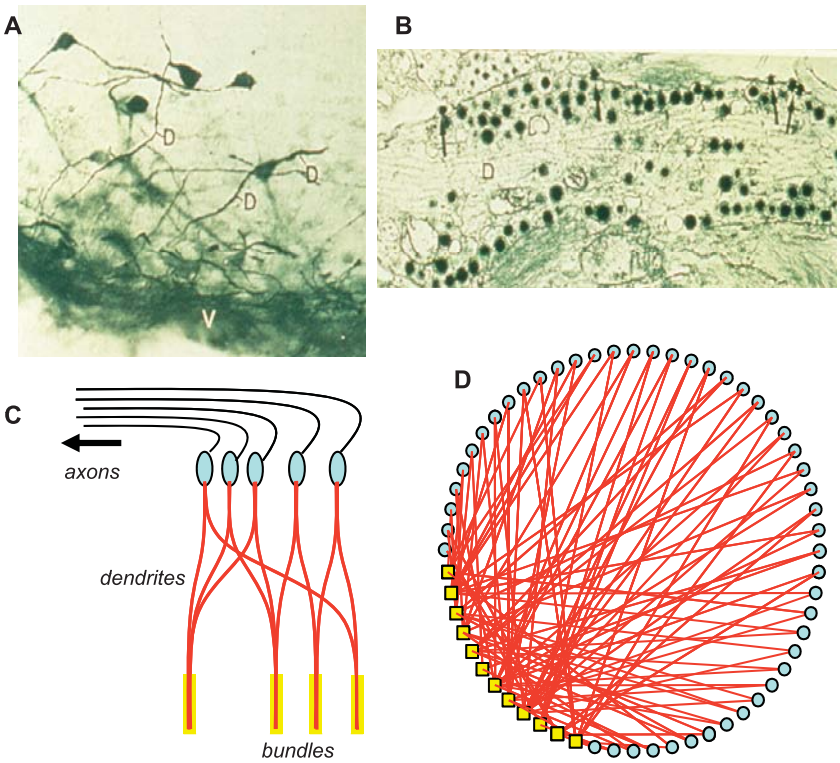

Figure 5 Structure of the model network Oxytocin cells in the supraoptic nucleus have 1-3 large dendrites, most of which project ventrally (shown by immunocytochemistry in **A**. These dendrites many neurosecretory vesicles (shown by electron microscopy in **B**). In the model, cells (**C**, blue) have two dendrites (red) that are coupled within bundles (yellow). The organization of the oxytocin network is shown in **D**; the yellow boxes represent dendritic bundles.

where k_τ is the maximum fraction of the pool that can be released by a spike, Δ is a fixed delay before release, and the summation extends over the set $\{t_i^s < t, t_i^s - t_i^{s-1} < \tau_{rel}\}$, with τ_{rel} a constant. Thus, only spikes occurring at intervals of less than τ_{rel} induce any release from dendrites. We set $\tau_{rel} = 50$ ms, but the exact value is not critical.

Modelling the effects of endocannabinoids

The variables $\epsilon_k(t), k = 1, ..., n_b$ represent the concentration of endocannabinoids in each bundle, and evolve according to

$$\frac{d\epsilon_k}{dt} = -\frac{\epsilon_k}{\tau_{EC}} + k_{EC} \sum_{i=1}^{n} \sum_{j=1}^{2} c_{ij}^k p_i^j \qquad (9)$$

where τ_{EC} is the decay time constant, and k_{EC} scales the amount of oxytocin released within the bundles into an increase of endocannabinoid concentration. The rates of EPSPs and IPSPs are equally affected by endocannabinoids:

$$\lambda^j_{x,i}(t) = [1-\alpha \sum_k c^k_{ij} F_{att}(\epsilon_k)]\overline{\lambda}^j_{x,i}(t) \tag{10}$$

where $\overline{\lambda}^j_{x,i}(t)$, $x = E,I$ are the unmodified synaptic input rates for dendrite j of neuron i, α is the maximal fractional attenuation of the input, and

$$F_{att}(\epsilon) = \frac{\epsilon^4}{\epsilon^4 + \epsilon^4_{th}} \tag{11}$$

where ε_{th} is a constant. The parameter values are given in Table 1 unless otherwise stated. The equations were integrated numerically by the Euler-Maruyama method with a time step of 0.1 ms. The MATLAB code for simulating the system is given in http://www.informatics.sussex.ac.uk/users/er28/otnet/.

Network topology (Figure 5)

The network has n neurons and n_b bundles, and each neuron has two dendrites in different bundles. To assign dendrites to bundles for a network of n neurons, and for an integer $d > 0$, we start by considering a set of $n_b = (2n/d)$ empty bundles. For each neuron we select two bundles as follows. The index of the first bundle (i_1) is selected at random from $\{1,2,\ldots,n_b\}$, the second index is selected at random from $\{1,2,\ldots,n_b\}/\{i_1\}$, ensuring that no neuron has two dendrites in the same bundle. This, repeated for all neurons, leads to a random allocation of dendrites into bundles.

Model behavior

Overview(Figures 6 & 7)

In the model, in the absence of a suckling input, cells fire spikes independently at a rate that depends on the level of synaptic input, and with interspike interval distributions very similar to those of oxytocin cells recorded *in vivo*. When the suckling input (k_p) is switched on, there is (at first) little change in this background activity, but there is progressive priming of activity-dependent oxytocin release, accompanied by production of endocannabinoids. As these begin to take effect, faster firing cells tend to slow down and slower firing cells tend to speed up. Then, after a delay, synchronised bursts arise throughout the network and recur every few minutes.

Table 1 Model parameters (a.u., arbitrary units)

Name	Description	Value	Units
n	Number of cells	48	
n_b	Number of bundles	12	
τ	Membrane time constant	10.8	ms
v_{rest}	Resting potential	−62	mV
$a_E(v_E - v_{\text{rest}})$	EPSP amplitude	4	mV
$a_I(v_{\text{rest}} - v_I)$	IPSP amplitude	4	mV
v_E	EPSP reversal potential	0	mV
v_I	IPSP reversal potential	−80	mV
$\bar{\lambda}_E$	Excitatory input rate	80	Hz
$\bar{\lambda}_I$	Inhibitory input rate	80	Hz
k_{HAP}	HAP, maximum amplitude	40	mV
τ_{HAP}	HAP, decay time constant	12.5	ms
k_{AHP}	AHP, maximum amplitude	40	mV
τ_{AHP}	AHP, time constant	2	s
f_{th}	AHP, half-activation constant	45	a.u.
τ_{OT}	Time decay of oxytocin-induced depolarization	1	s
k_{OT}	Depolarization for unitary oxytocin release	0.5	mV
Δ	Time delay for oxytocin release	5	ms
$T_{OT,max}$	Maximum oxytocin-induced depolarization	25	mV
k_p	Priming rate	0.5	s^{-1}
τ_r	Time constant for priming	400	s
k_r	Fraction of dendritic stores released per spike (max)	0.045	
τ_{EC}	Time constant for [EC] decay	6	s
k_{EC}	Endocannabinoid increase per unit oxytocin release	0.0025	a.u.
ϵ_{th}	[EC] threshold for synaptic attenuation	0.03	a.u.
τ_{rel}	Maximum interspike interval for release	50	ms
α	Fractional attenuation of synaptic input rate (max)	0.6	

Example simulations

Figure 8 shows simulations from a network of 48 neurons and 12 bundles (with a mean of 8 dendrites per bundle) with the topology as in Figure 6 (the results are similar in networks of up to 3000 neurons). Synchronized bursts occur when, and only when, the suckling input is present; i.e., priming of dendritic release is essential. The model parameters were tuned to match the interspike interval distributions of oxytocin cells and the temporal characteristics of bursts (Table 1). With these parameters, bursts contain 50-70 spikes in 1-3 s (0.9-4.6 s *in vivo*), and recur at intervals of ∼4 min, in close agreement with *in vivo* observations.

Interspike interval histograms (Figure 9) constructed between bursts match *in vivo* data indistinguishably, so the model accounts well for the background activity of the oxytocin cells, as well as bursting activity. Normally, all cells participate in the reflex in the model, and the mean variation in burst onset is about 200 ms, close to measurements

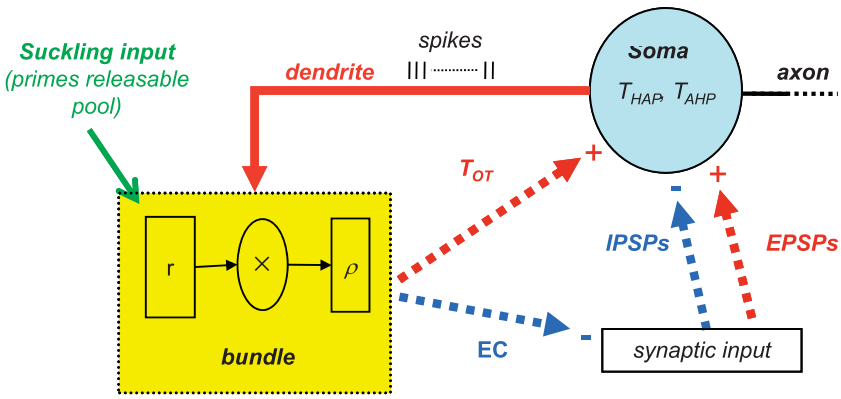

Figure 6 The structure of a single model neuron A single model neuron receives random EPSPs and IPSPs, and its excitability is modelled as a dynamically changing spike threshold that is influenced by a HAP (parameter T_{HAP}), and a slower AHP (T_{AHP}). Each neuron interacts with neighbouring neurons by two dendrites that project to bundles (yellow), and its excitability is increased when oxytocin is released in these bundles (T_{OT}). Activity-dependent production of endocannabinoids (*EC*) feeds back to reduce synaptic input rates.

in vivo. Model neurons display a brief silence *before* many bursts; in the model, endocannabinoids released from the first cells that burst can suppress synaptic input enough to inhibit other oxytocin cells before they are activated by oxytocin release, and similar pre-burst silences occur *in vivo*.

Roles of the HAP and AHP

In the model, the shape of bursts is determined by the AHP, which reduces the peak firing rate and shortens the burst duration. Removing the AHP has little effect on the timing of bursts, as it activated relatively little at background firing rates.

The HAP parameters were fixed to provide a good match to the interspike interval distribution between bursts. The choice of parameters affects the timing of bursts, as the HAP limits the occurrence of short interspike intervals; more short intervals increases the rate of depletion of dendritic oxytocin, but also increases the frequency of events that can trigger a burst.

Pacemaker activity

As *in vivo* there are no fixed 'leader' or 'follower' cells in the network, and the order in which neurons start to burst varies randomly with each burst. Bursting in the model is thus an **emergent activity** due to the interplay between the single neuron dynamics and network dynamics. The lack of a marked leader/follower character is accentuated by the homogeneous arrangement of the connections in the network, as all bundles contained the

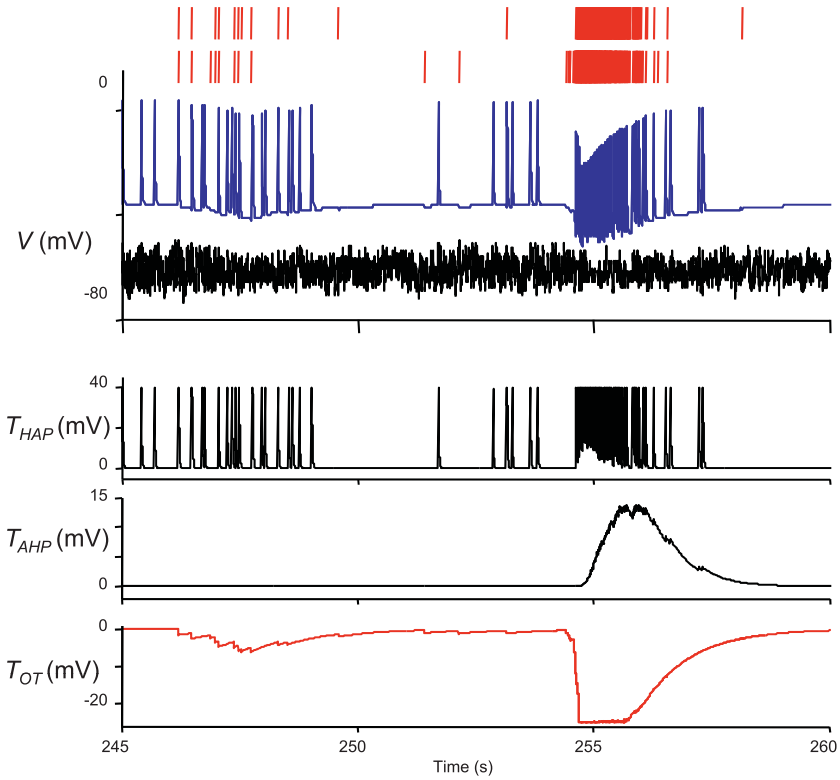

Figure 7 The behavior of one model cell during a burst. The upper two red traces show the times of occurrence of all oxytocin release events in the two dendritic bundles to which the cell is connected. Below this is the soma activity: the blue line shows the spike threshold, showing the effects of post-spike activity changes and of oxytocin; the black line (*V*) shows the impact of EPSPs and IPSPs. The bottom three traces show T_{HAP}, T_{AHP} and T_{OT}.

same number of dendrites. We also considered a network with the same number of cells and bundles (and the same mean connectivity) but where the number of dendrites varied in each bundle, and in this, bursts are more likely to start in regions of the network where dendritic bundling is more pronounced.

Synchronization

With no suckling input, the firing of oxytocin cells in the model is uncorrelated (as *in vivo*). Between bursts, spiking activity is characterised by small but increasing cross-correlation of firing rates, a consequence of the strengthening of the interactions between cells. Activity becomes more irregular close to a burst, indicated by an increasing index of dispersion of the firing rate. Both results agree with experimental findings *in vivo*. In the model, the increased variability arises because, towards a burst, activity produces both dendritic oxytocin release, with excitatory consequences, and endocannabinoid production, with inhibitory consequences. If

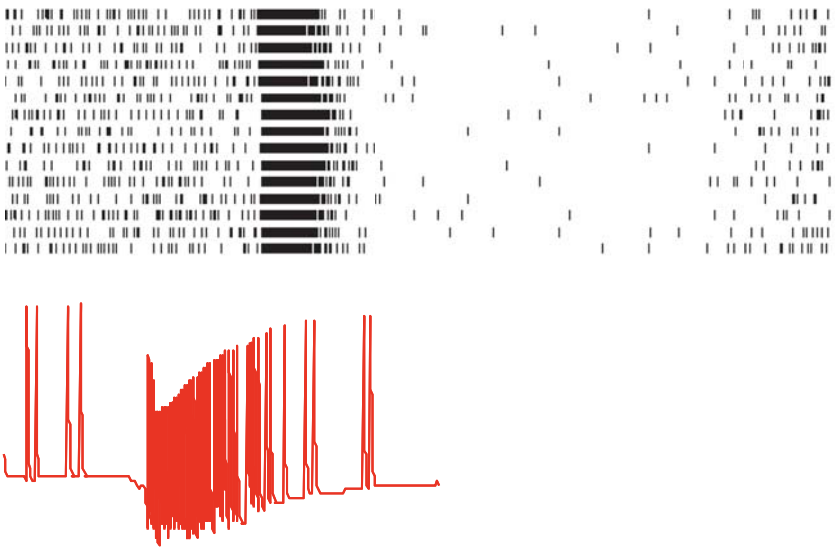

Figure 8 Synchronized bursting in model oxytocin cells Each row of the raster shows the spike activity of just one of the 348 cells in a network model; each bar shows the timing of a spike. Bursts are approximately synchronized, while background activity is asynchronous. The red trace below shows how T changes during a burst in one of the cells; each spike causes a large transient rise in T. As oxytocin is released, this causes a fall in T that is offset by a slow rise caused by the AHP. Note how similar this profile is to the extracellularly recorded voltage trace of oxytocin cells in Figure 1.

endocannabinoid release is eliminated (by setting $\alpha = 0$) then there is no increase in variability.

In a network of 1000 neurons with just two dendrites in each bundle, bursts are rare, propagate slowly, and involve only some cells. More dendrites in each bundle leads to faster propagation of bursts and better synchronization. Figure 10 illustrates how a burst is propagated between cells, and shows the effects of varying the degree of random connectivity. With random coupling, large networks can be rapidly synchronized even if the coupling is sparse. If cells are coupled less randomly (i.e. more regularly), synchronization is poorer and "travelling waves" can arise.

Post-Burst silences

Bursts are followed by long silent periods (up to 20 s), very similar to post-burst silences *in vivo*. *In vivo*, the silence is variable in duration (7-56 s), indicating that it is not simply the deterministic consequence of an activity-dependent AHP. In the model, the post-burst silence is mainly a consequence of the prolonged suppression of afferent input, following the increase in endocannabinoids. *In vivo*, a few otherwise typical oxytocin cells show no bursts at milk ejection but instead fall silent. A similar

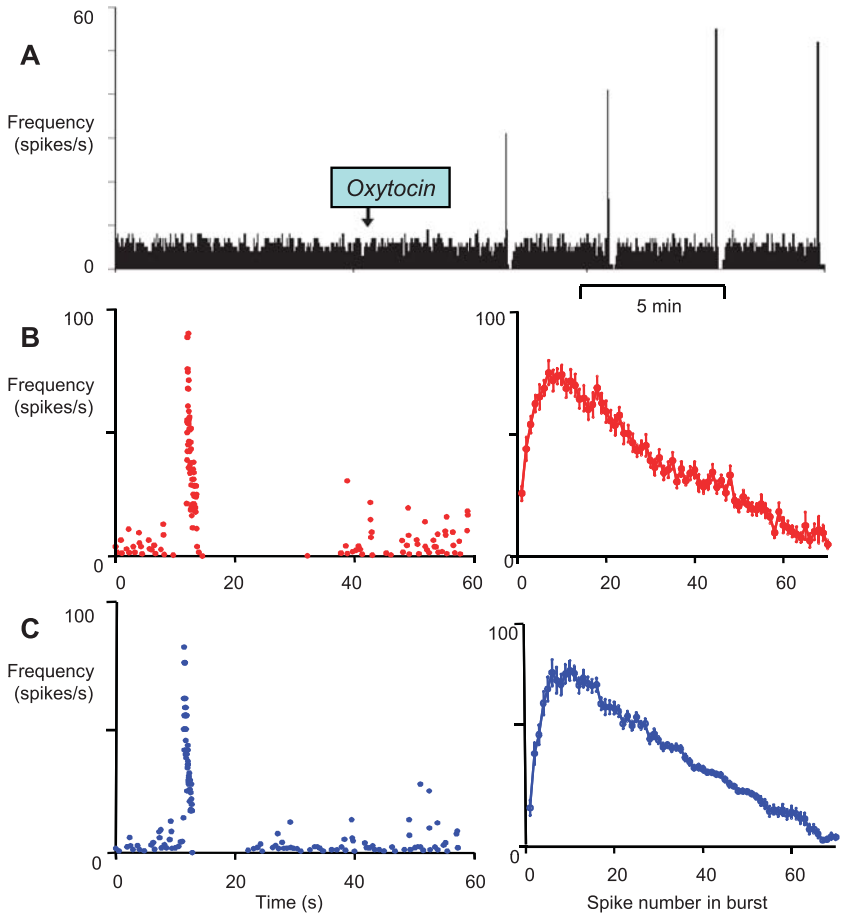

Figure 9 Comparison of bursting activity in real and modelled oxytocin cells
A. Milk-ejection bursts triggered in an oxytocin cell *in vivo* by i.c.v. injection of oxytocin in a urethane-anaesthetised rat. **B**. A milk-ejection burst in an oxytocin cell recorded *in vivo* (red) and a model cell (blue) plotted as instantaneous firing rate (each point is the reciprocal of the interval since the previous spike). This profile is indistinguishable to burst profiles observed *in vivo*. **C**: Mean profiles of milk-ejection bursts from a real oxytocin cell (red) (Data file) and from a model cell (blue). Each profile is constructed from 17 bursts, and shows the mean (± S.E.) instantaneous firing rate plotted for each interspike interval within the bursts

phenomenon can be replicated in the model by assuming that some neurons do not express oxytocin receptors (by setting $k_{OT}=0$ for these neurons).

Dendritic storage

In the model, the dendritic stores of readily-releasable vesicles are incremented by the suckling input. Their average level increases between bursts

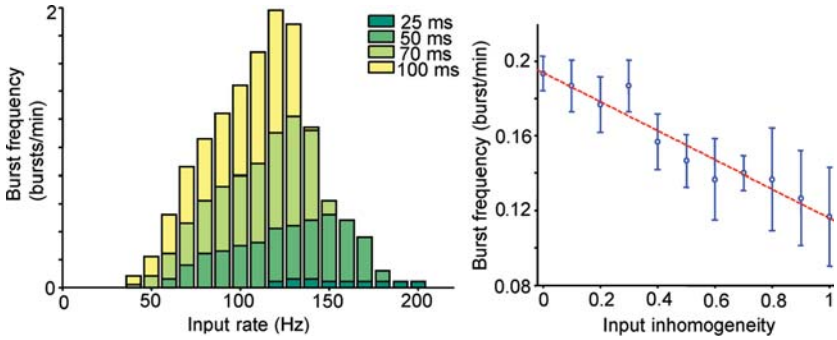

Figure 10 Dependence of bursting on synaptic input (**Left**) In simulations of the model network, bursting behaviour is observed only within a range of values for the excitatory input. A minimum level of excitation is necessary to start the reflex. Increasing the input rate speeds up bursting until the excess of oxytocin release causes an abrupt breakdown. Bar colours correspond to varying the threshold for frequency-dependent release, defined as the maximum interspike interval allowed for dendritic release. (**Right**) The effect of a spatially inhomogeneous input on bursting activity. Cells were subject to (balanced) inputs of rate $\lambda = \lambda_0(1 + \varepsilon)$, with ε drawn from a normal distribution. Plotted is the bursting frequency (based upon 50 min of dynamics; average over five trials with independently distributed rates) vs the SD of ε. Bars are SD; the dashed line is a linear fit.

despite activity-dependent depletion, and bursts tend to occur when the stores are relatively large. The mean level at the time of bursts correlates strongly with the logarithm of the inter-burst interval. Figure 11 plots the rate of change of the stores against the store level. The decrease in slope at high levels reflects a reduction of the average release rate, and is a consequence of the suppression of afferent input as a result of endocannabinoid release. This stops release from becoming regenerative, and allows the stores to increase further. In this phase, the network activity becomes more irregular because of the opposing feedback mechanisms: local activity-dependent excitation by dendritic oxytocin release, and suppression of afferent input by endocannabinoids. If just a few neighbouring cells show coincidentally increased activity due to stochastic variation in their input rates, and if they have large enough stores, then enough oxytocin can be released to trigger a burst.

Paradoxical behaviors

Increased spike activity between bursts enhances depletion of the readily-releasable pool and so can delay or even suppress bursting. Conversely, an increase in inhibitory input can promote the reflex in a system which fails to express bursting because of insufficient priming (Figure 10). Such "paradoxical" behaviours have been extensively described *in vivo*; for example, injections of the inhibitory neurotransmitter GABA into the

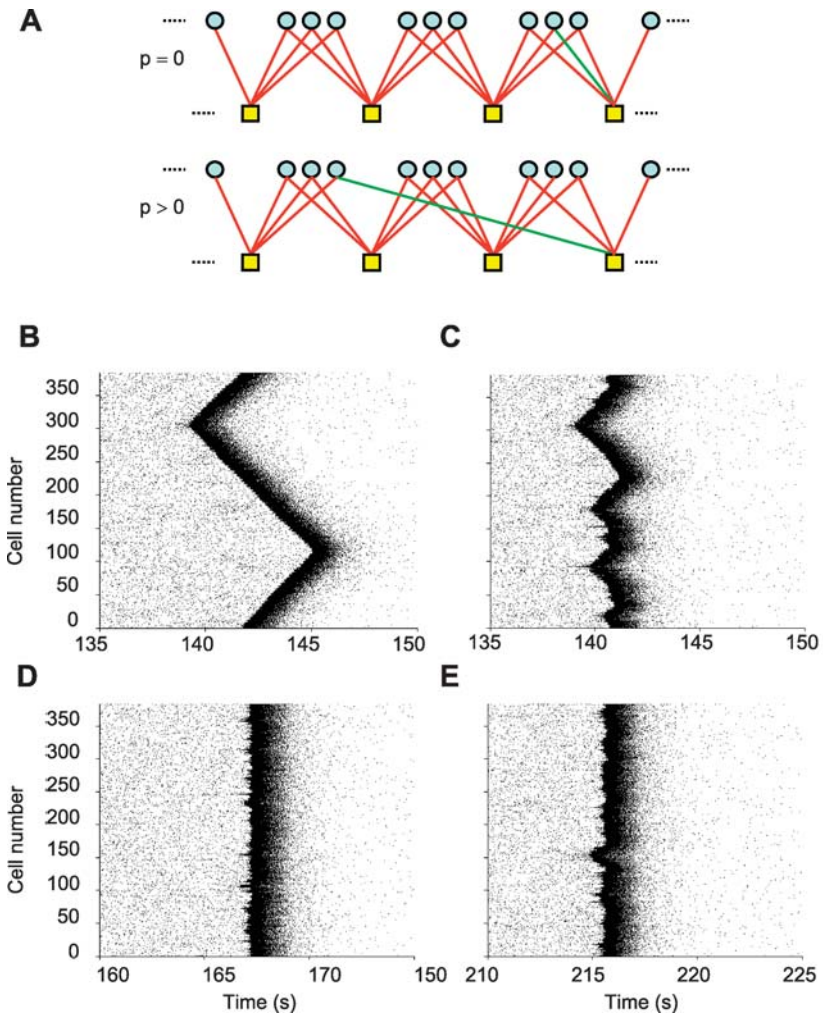

Figure 11 Impact of network topology on the propagation of bursting. The network topology is critical for whether bursting is synchronous, or whether it occurs as a travelling wave through the network. A, Schematic diagram illustrating a network with a ring structure ($p = 0$, top) and with random rewiring ($p > 0$, bottom); blue circles indicate neurons, yellow boxes indicate bundles. One dendrite (in green) is randomly chosen and re-assigned; this is shown for only one neuron but the rule was applied to all neurons independently. B-E, Raster plots of spikes generated in networks with increasing probability of rewiring: $p = 0$ (B), 0.05 (C), 0.5 (D), 0.95 (E).

supraoptic nucleus of a suckled, lactating rat can trigger milk-ejection bursts; conversely, many stimuli that activate oxytocin cells suppress the reflex. Occasionally a single burst can occur shortly *after* removing the suckling stimulus. This feature is also shared (occasionally) by the reflex *in vivo*, and indicates that suckling itself is not a strictly necessary trigger.

Network structures

In the model, during suckling, neurons that are strongly excited produce endocannabinoids that reduce the overall input level. This defends the system from over-excitation, and maintains the network in an optimal range for bursting. This is important, because bursting is possible only within a range of values of synaptic input. The exact range depends on the strength of the coupling between spike activity and dendritic secretion. At a low level of excitation, an increase in synaptic input favours bursting by increasing the frequency of release episodes which can trigger a burst. However, above a critical level, such release events may be so frequent that stores are not replenished fast enough for the stores to reach the critical level required to trigger a burst. Bursts become rarer and less predictable, until eventually over-excitation disrupts the reflex. Spatial inhomogeneity in the stochastic input can also degrade the reflex. The system performs optimally when the activity is relatively homogeneous between oxytocin cells, a conclusion previously drawn from experimental studies.

Discussion

During lactation, oxytocin is released in pulses following quasi-synchronous bursts of spike activity in oxytocin cells. Here, computer-based modelling shows that such bursting can arise as an emergent property of a spiking neuronal network. The model does not incorporate all elements of the physiology of oxytocin cells, but is a minimalist representation to help identify the key processes.

Key model assumptions

In formulating this model, we are hypothesising that, during lactation, the oxytocin system is organized as a pulse-coupled network where neurons interact by dendritic release of oxytocin, coupled non-linearly to electrical activity. This requires a stimulus-dependent process of *priming* of the dendritic stores, whereby these are made available for activity-dependent release. Dendritic release of oxytocin occurs only when the neuron's firing rate is sufficiently large, so interactions between neurons are rare and erratic between bursts and in the absence of the suckling stimulus, leading to asynchronous spiking except during the bursts themselves; the network is essentially thus a *pulse-coupled network*.

Emergent behavior

In this model, bursting arises as an *emergent behaviour* of a sparsely connected population of neurons. Bursting can begin at any of many foci of neuronal interactions – within any of the dendritic bundles that link just a few of the

neurons, from where it will spread out to the remaining bundles. Bursting arises by positive feedback through activity-dependent release of oxytocin, and this is down-regulated after a burst (by depletion of the pool of readily-releasable oxytocin); the core mechanism is thus analogous to a mechanism used in some other models of bursting – positive feedback followed by synaptic depression. The topology of the networks is different – the present network is sparsely connected compared to others, and the biological substrate is different – here the intercommunication is dendro-dendritic rather than synaptic.

Making biological inferences from the model

Matching the model to data helps us to understand the likely importance of several biological phenomena. First, the AHP has a role only in shaping the burst profile; it contributes little to burst timing or to post-burst silences. Second, although the core mechanism inducing bursts is activity-dependent positive feedback, negative feedbacks also are also important. In the real system there are many negative feedback mechanisms involving several signalling molecules, here these are represented by only one – the endocannabinoids, and this is an oversimplification. In the model, endocannabinoid production is proportional to oxytocin release. The dynamics of the effects of endocannabinoids differ from those of oxytocin, and the dual effects promote increased variability in firing rate as the system swings from excitation to inhibition. The "upswings" mean that, for a given mean firing rate, there are more clusters of short intervals towards the end of an interburst interval, and they are more likely to be correlated between neurons, making them more potent as potential burst-triggering events. At the same time, the depressive effects on mean firing rate means that at high synaptic input rates there is less depletion of the releasable pool of oxytocin. Together, these effects mean that the rate at which bursts arise is relatively independent of synaptic input rate over a reasonably wide range.

New questions that arise from the model

The model makes it possible to study how bursting behaviour relates to network connectivity. Mathematically, the network can be described by a *bipartite graph*$G = \{NUB, E\}$, where N is the set of neurons, B the set of bundles, and E the set of connections from neurons to bundles such that, for neuron a in N and bundle b in B, $(a, b)\epsilon E$ if a has a dendrite in b (Figure 12) The network topology is specified by $\mathbf{O} = \{o_{ij}\}$, $i = 1,\ldots, n$, $j = 1,\ldots,n_b$, where $o_{ij} = 1$ if neuron i has a dendrite in bundle j, and $o_{ij} = 0$ otherwise. If dendro-dendritic connections are formed at random, then $\mathbf{O}$ is a random binary matrix whose rows satisfy $\sum o_{ij} = 2$. From the graph $G = \{NUB, E\}$ we can derive the graphs $G_N = \{N, E_N\}$ and $G_B = \{B, E_B\}$ for connections between the neurons and the bundles respectively. The *edge set* of G_N, E_N contains all

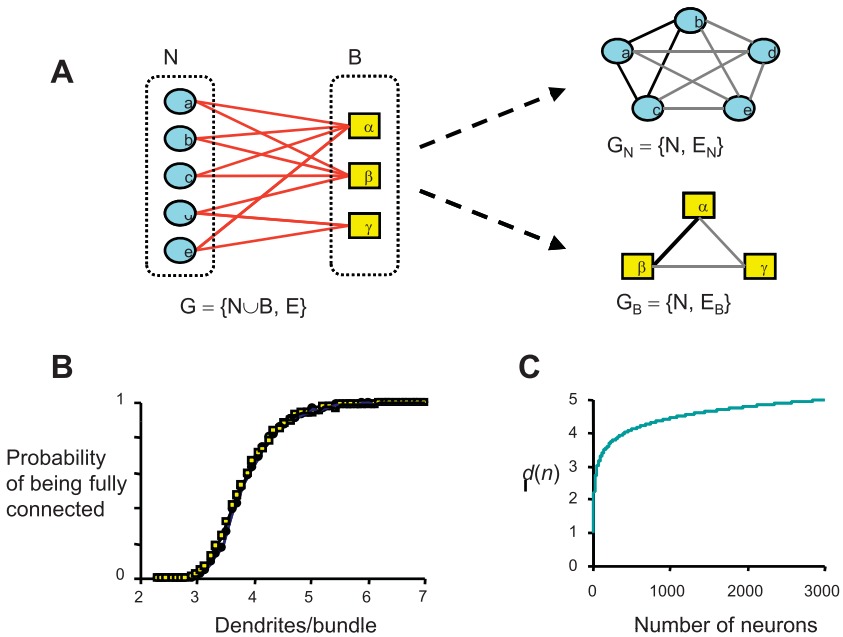

Figure 12 How bursting behaviour relates to network connectivity. A The network can be described by a *bipartite graph*, where N is the set of neurons, B the set of bundles, and E the set of connections from neurons to bundles such that, for neuron a in N and bundle b in B, if a has a dendrite in b. From these graph we can derive graphs G_N and G_B for connections between the neurons and the bundles respectively.For the network to be collectively activated during a burst it must be *connected*, i.e. any two neurons must be connected by some path. B plots the probability that a network of 1000 cells with two dendrites/cell will be fully connected for different numbers of dendrites per bundle, above a critical value of about 4.5 the network is almost certainly fully connected. C shows how the critical value is affected by the number of neurons in the network.

pairs of neurons which share at least one bundle, while the edge set of G_B, E_B contains all pairs of bundles which are 'bridged' by at least one neuron. For G_B, the *node degrees* represent the number of dendrites in the corresponding bundles, i.e. $d_j = \sum o_{ij}, . j = 1, \ldots, n_b$. If the bundles are formed at random, the latter form a set of identically distributed random variables of mean $\bar{d} = 2n/n_b$. The average number of connections formed by each neuron can then be estimated as $2(\bar{d}-1)$.

For the network to be collectively activated during a burst it must be *connected*, i.e. any two neurons must be connected by some path. The probability that the network is connected can be estimated by approximating G_N (or G_B) with a random graph of same size and average degree; a random graph of n nodes is almost certainly connected if its average degree is $\geq \log n$, suggesting that a network of n neurons will be connected if $\bar{d} \geq 1 + \frac{1}{2}\log n$. However, the oxytocin network has different topological

properties, so we compared the fraction of connected networks in a sample of 1000 random networks and 1000 approximating random graphs, with varying $\bar{d}$. For each value of $\bar{d}$ we considered a set of n neurons and $n_b^0 = 2n/\bar{d}$ bundles. Then, for each neuron i we chose (uniformly at random) two bundles of indices (i_1,i_2), $i_1, i_2 = 1, ..., 2N/\bar{d}$,, $i_1 i_2$, and set $o_{ij1} = o_{ij2} = 1$. Finally, bundles with no dendrites were removed from the bundle set. The result is a graph of n neurons and $n_b = n_b^0 - n_b^{(e)}$ bundles, where $n_b^{(e)}$ is the number of empty bundles. The mean number of dendrites per bundle was then recomputed as $\bar{d} = 2n/n_b$. We calculated the average degree of the resulting network and then generated a random graph with the same average degree. We confirmed the validity of the approximation with a network of 1000 neurons (which is about as many as there are oxytocin cells in one supraoptic nucleus). Figure 12 plots the critical value of $\bar{d}$ for the random graph; the predicted value for $n = 1000$ is 4.45. When $\bar{d}$ is larger than this, more than 85% of the generated networks are fully connected. This result is in accord with the empirically observed connectivity of oxytocin cells (oxytocin cells have 1-3 dendrites in bundles of 3-8 dendrites).

Model topology and wave propagation

The topology of the oxytocin network is important for both the generation and the synchronization of bursts. The interconnections within bundles, combined with the excitatory effect of oxytocin, lead to a positive feedback which sustains burst generation. At the same time, random connections between bundles reduce the typical path length between any two neurons of the network, enhancing synchronization.

We studied a network of 384 neurons with dendrites in 96 bundles using a different, *ring* topology. Here, neurons are grouped in clusters, those in a given cluster project to the same two bundles, and each bundle receives dendrites only from two adjacent clusters, forming a chain-like structure. This is equivalent to assuming that neurons preferentially contact their closest neighbours. In this network, bursting is *not* synchronized; two wave fronts travel along the network and it takes ~5 s for a burst to be propagated across the whole network. Figure 11 shows the results in networks with increasing probability of rewiring p. Starting from the ring topology, we randomly rewired one dendrite for each neuron with probability p. As the probability of rewiring increases (i.e. with more random connectivity), bursts become progressively more synchronized. Thus, the bursting synchronization is sensitive to the network topology, and is observable with a *small-world* type topology.

Bursting, spiking and multiscale dynamics

Whereas neurons exchange information mostly via spikes, endocrine cells rely on hormonal pulses to signal to their target tissues. For many

neurons, clustered spike activity can be optimally effective in inducing the required changes on the targets, but for endocrine cells to generate a signal large enough to be read at a distance, their secretory activity must not only be optimal for each cell, their activity must also be co-ordinated; hence peptide hormone signals are generally pulsatile. Many neurons in the brain produce a peptide as well as a conventional transmitter, and many peptides have effects on organismal behaviour that are hormone-like, in that they act at dispersed and distant targets to produce prolonged organisational changes. For a hormone-like, pulsatile signal to be produced reliably, the activity of a population of peptide-secreting neurons must be co-ordinated in a physiologically plastic manner. In the present model, network interactions are solely mediated by spikes with interspike intervals less than τ_{rel}; similar spike doublets are thought to play a critical role in the synchronization of network activity in many neural systems.

Limitations of the model

The present model produces a close match to electrophysiological data, and its strength is the simplicity of the core representation of a single neuron; this makes it possible to explore how properties of the network, affect the system behaviour. The simplifications that we made in modelling the reflex are mainly unlikely to have had any major influence, with two possible exceptions. First, we have not included intracellular [Ca^{2+}] changes as a variable, although we know that mobilisation of intracellular Ca^{2+} stores can trigger dendritic oxytocin release, and therefore probably contributes to oxytocin release during milk-ejection. Implicitly we assumed that this overlaps with activity-induced oxytocin release and hence can be neglected, but in some circumstances oxytocin release triggered by Ca^{2+} release from intracellular stores might precipitate a burst. Second, we modelled dendritic release as a relatively common deterministic event. In fact, dendritic release probably occurs as the relatively rare exocytosis of large vesicles that each contain a large amount of oxytocin (about 85,000 molecules) – and the release process is likely to be stochastic, with interval length governing the probability of release rather than determining it. Whether this will affect the model behaviour substantially remains to be tested.

Perspectives

The model described here is a "systems level model." It describes the behavior of a complex system in a concise way; it does not include representations of the full level of detail that is known, but it tests our

understanding of the ways in which particular qualitative behaviors arise. A system, in this sense, is just an arrangement of circumstances that makes things happen in a certain way. We look to model something that has a defined, and measurable input and output, that are connected by known or hypothesised rules. This could be a signalling pathway within a single cell, but often we apply the 'systems' tag to things that involve higher level processing, with multiple components, many of which may be unknown. The purpose of such modelling can be said to be to generate hypotheses about the types of processing that take place, and about how it might be organized.

In this case, the *measurable output* is the spike activity observed in oxytocin cells during suckling. These derive from extracellular recordings, so while we know much about spike generation in oxytocin cells from *in vitro* recordings, there is little to be gained by a fully biophysical model of oxytocin cells because we have no intracellular recordings of the bursting activity of oxytocin cells with which to compare the model performance. There is little point in generating predictions about things that cannot be measured, and which depend upon assumptions that involve dubious extrapolations from data derived under conditions that deviate in uncertain ways from the situation to be modelled.

Even the present model displays outcomes that would have been hard to predict and are correspondingly hard to explain; the more detailed a model is, the harder it is to understand *why* it does what it does. If the aim of a model is to test the completeness and limitations of our understanding, it is important to build a model that can be understood, and amenable to systematic investigation. The more parameters that a model has, the harder it is to systematically study its behavior – and these difficulties increase exponentially with the number of free parameters. Keeping models simple is essential for making them useful.

Glossary

The **supraoptic nucleus** is an aggregation of magnocellular neurosecretory neurons that, on both the left and right side of the brain, is located at the ventral surface of the brain directly adjacent to the rostro-lateral edge of the optic chiasm. The nucleus contains just two types of neuron, oxytocin neurons and vasopressin neurons, all of which project a single axon to the posterior pituitary gland.

The **Heaviside step function**, H, has a value of zero for a negative argument and one for a positive argument. It is used to represent a signal that switches on at a specified time and stays on indefinitely.

The **Dirac delta** $\delta(x)$, used to model a tall narrow 'spike' function, is zero everywhere except at $x = 0$ where its value is infinitely large, so that its total integral is 1. It can be viewed as the derivative of the Heaviside step function.

A **small-world network** is a graph in which most nodes are not neighbors of each another, yet most nodes can be reached from any other node by a small number of steps (i.e. via a short chain of mutual acquaintances).

A **bipartite graph** is one whose vertices can be divided into two disjoint sets such that every edge connects a vertex in one of the sets to a vertex in the other.

Endocannabinoids are "endogenous cannabinoids": molecules that act at specific cannabinoid receptors (in this case CB1 receptors). CB1 receptors are widely expressed in the brain, often on nerve endings. Cannabinoids are produced in some neuronal populations in response to raised intracellular calcium, and act on afferent nerve endings that express these receptors to inhibit transmitter release; cannabinoids are thus *retrograde transmitters*.

In vitro preparations here refer to electrophysiological studies of supraoptic neurons in a hypothalamic slice preparation.

The neurosecretory **vesicles** are (relatively) large membrane bound vesicles tightly packed with oxytocin (and other fragments of the precursor protein from which oxytocin is cleaved). Each contains about 85,000 molecules of oxytocin. The tight packing of the peptides mean that under the electron microscope, these vesicles have an electron-dense core, and so these are often referred to as "large dense-cored vesicles" to distinguish them from the small clear synaptic vesicles in which conventional neurotransmitters, such as glutamate and GABA, are packaged.

Dataset 1

Excel file giving raw data of spike times from thirteen successive milk-ejection bursts recorded from a single oxytocin cell in a urethane-anaesthetised rat, from the experiments reported by Dyball and Leng (1987). Each cell entry is the instantaneous frequency (the reciprocal of the interspike interval for successive interspike intervals), and each column records a single burst. The yellow areas highlight pre-burst activity; the bursts are aligned to the first occurrence of an interspike interval of < 100 ms in a long sequence of short intervals.

Bibliography

Essential references

Rossoni E, Feng J, Tirozzi B, Brown D, Leng G, Moos F (2008) Emergent synchronous bursting of oxytocin neuronal network. *PLoS Comput Biol* 4.(7) http://www.ploscompbiol.org/article/info%3Adoi%2F10.1371%2Fjournal.pcbi.1000123

First report of the milk-ejection burst model

Leng G, Brown CH, Bull PM, Brown D, Scullion S, Currie J, Blackburn-Munro RE, Feng J, Onaka T, Verbalis JG, Russell JA, Ludwig M (2001) Responses of magnocellular neurons to osmotic stimulation involves co-activation of excitatory and inhibitory input: an experimental and theoretical analysis. *J Neurosci* 21: 6967–77.

Account of the integrate-and fire model as first applied to oxytocin cells

Ludwig M, Sabatier N, Bull PM, Landgraf R, Dayanithi G, Leng G (2002) Intracellular calcium stores regulate activity-dependent neuropeptide release from dendrites. *Nature* 418: 85–9.

First account of priming of dendritic oxytocin release

Hirasawa M, Schwab Y, Natah S, Hillard CJ, Mackie, Sharkey KA, Pittman QJ (2004) Dendritically released transmitters cooperate via autocrine and retrograde actions to inhibit afferent excitation in rat brain *J Physiol* 59: 611–24.

Key paper on actions of endocannabinoids

Key reviews of the biological background to the milk-ejection reflex

Leng G, Brown D (1997) The origins and significance of pulsatility in hormone secretion from the pituitary *J Neuroendocrinol* 9: 493–513.

Ludwig M, Leng G (2006) Dendritic peptidic release and peptide dependent behaviours. *Nat Neurosci Rev* 7: 126–36.

Leng G, Brown CH, Russell JA (1999) Physiological pathways regulating the activity of magnocellular neurosecretory cells. *Prog Neurobiol* 57: 625–55.

Russell JA, Leng G, Douglas AJ (2003) The magnocellular oxytocin system. *The fount of maternity: adaptations in pregnancy Front Neuroendocrinol* 24: 27–61.

Theodosis DT (2002) Oxytocin-secreting neurons: A physiological model of morphological neuronal and glial plasticity in the adult hypothalamus Front *Neuroendocrinol* 23: 101–35.

Leng G, Ludwig M (2006) Information processing in the hypothalamus: Peptides and analogue computation *J Neuroendocrinol* 18: 379–92.

Source papers for key biological data on the milk-ejection reflex

The two papers below, by Jonathan Wakerley and Dennis Lincoln, were the first descriptions of the milk-ejection reflex.

Wakerley JB, Lincoln DW (1973) The milk-ejection reflex of the rat: a 20- to 40-fold acceleration in the firing of paraventricular neurones during oxytocin release. *J Endocrinol* 57: 477–93.

Lincoln DW, Wakerley JB (1974) Electrophysiological evidence for the activation of supraoptic neurons during the release of oxytocin. *J Physiol* 242: 533–54.

The papers below, from the laboratory of Francoise Moos, describe various quantitative aspects of milk-ejection bursts.

Brown D, Moos FC (1997) Onset of bursting in oxytocin cells in suckled rats *J Physiol* 503: 625–34.

Moos FC, Fontanaud P, Mekaouche M, Brown D (2004) Oxytocin neurones are recruited into co-ordinated fluctuations of firing before bursting in the rat. *Neuroscience* 125: 593–602.

Brown D, Fontanaud P, Moos FC (2000) The variability of basal action potential firing is positively correlated with bursting in hypothalamic oxytocin neurones *J Neuroendocrinol* 12: 506–20.

Belin V, Moos FC (1986) Paired recordings from supraoptic and paraventricular oxytocin cells in suckled rats: recruitment and synchronization *J Physiol* 377: 369–90.

The papers below are a small selection of experimental studies displaying key features of the reflex

Lambert RC, Moos FC, Richard P (1993) Action of endogenous oxytocin within the paraventricular or supraoptic nuclei: A powerful link in the regulation of the bursting pattern of oxytocin neurons during the milk-ejection reflex in rats *Neuroscience* 57: 1027–38.

Wang YF, Hatton GI (2004) Milk ejection burst-like electrical activity evoked in supraoptic oxytocin neurons in slices from lactating rats. *J Neurophysiol* 91: 2312–21.

Lambert RC, Dayanithi G, Moos FC, Richard P (1994) A rise in the intracellular Ca^{2+} concentration of isolated rat supraoptic cells in response to oxytocin *J Physiol* 478: 275–88.

Dyball REJ, Leng G (1986) The regulation of the milk-ejection reflex in the rat *J Physiol* 380: 239–56.

Moos FC (1995) GABA-induced facilitation of the periodic bursting activity of oxytocin neurons in suckled rats *J Physiol* 488: 103–14.

Related theoretical papers

Albert R, Barabási AL (2002) Statistical mechanics of complex networks. *Rev Mod Phys* 74: 47–97.

De Schutter E, Maex R (1998) Synchronization of Golgi and granule cell firing in a detailed network model of the cerebellar granule cell layer. *J Neurophysiol* 80: 2521–37.

Leng G, Macgregor D (2008) Mathematical modelling in neuroendocrinology *J Neuroendocrinol* 20: 713–8.

Shao J, Tsao T, Butera RJ (2006) Bursting without slow kinetics: a role for a small world? *Neural Comput* 18: 2029–35.

Kopell N, Karbowski J (2000) Multispikes and synchronization in a large neural network with temporal delays. *Neural Comput* 12: 1537–606.

Whittington MA, Kopell N, Ermentrout GB (2000) Gamma rhythms and beta rhythms have different synchronization properties. *Proc Natl Acad Sci USA* 97: 1867–72.